METRICA
METRology Institutional CAtalog

ISTITUTO NAZIONALE DI RICERCA METROLOGICA
Repository Istituzionale

The linkup of mono-elemental solutions to the SI using INAA: a measurement procedure and the achievable uncertainty

(Article begins on next page)

25 November 2024

1 # Title page

2 Names of the authors: Giancarlo D'Agostino[1], Luigi Bergamaschi[1], Marco Di

3 Luzio[1,2], Janine Noordmann[3], Massimo Oddone[2] and Olaf Rienitz[3]

4 Title: The linkup of mono-elemental solutions to the SI using INAA: a measurement

5 procedure and the achievable uncertainty

6 Affiliation(s) and address(es) of the author(s): (1) Istituto Nazionale di Ricerca

7 Metrologica (INRIM) - Unit of Radiochemistry and Spectroscopy, c/o Department of

8 Chemistry, University of Pavia, via Taramelli 12, 27100 Pavia, Italy; (2) Department of

9 Chemistry – Radiochemistry Area, University of Pavia, via Taramelli 12, 27100 Pavia,

10 Italy; (3) Physikalisch-Technische Bundesanstalt (PTB), Bundesallee 100, 38116

11 Braunschweig, Germany

12 E-mail address of the corresponding author: g.dagostino@inrim.it

13

The linkup of mono-elemental solutions to the SI using INAA: a measurement procedure and the achievable uncertainty

D'Agostino G.[1], Bergamaschi L.[1], Di Luzio M.[1,2], Noordmann J.[3], Oddone M.[2] and Rienitz O.[3]

[1]*Istituto Nazionale di Ricerca Metrologica (INRIM), via Taramelli 12, 27100 Pavia, Italy*

[2]*Department of Chemistry, University of Pavia, via Taramelli 12, 27100 Pavia, Italy*

[3]*Physikalisch-Technische Bundesanstalt (PTB), Bundesallee 100, 38116 Braunschweig, Germany*

Abstract

The possibility of using neutron activation analysis to link up a secondary to a primary mono-elemental solution was investigated. A procedure was developed for the determination of the ratio between the mass fractions of two solutions. The use of a monitor element was essential to limit the effect of the non-uniformity of the neutron flux during irradiation. The proposed procedure was tested in the case of two molybdenum solutions having the same mass fraction. Although the experiment did not reach the goal, possible ways are suggested to reach the target expanded uncertainty of 0.1 %.

Keywords

Neutron activation analysis; metrological traceability; reference solution; molybdenum.

Introduction

34   Mono-elemental solutions with a mass fraction of 1 g kg^{-1} are being used in almost every

35   chemical laboratory in social, medical and industrial fields to calibrate analytical

36   measurements. The accuracy of those solutions is essential for the reliability and

37   comparability of the applied analyses.

38   Due to the importance of these calibration solutions, traceability to the SI is necessary.

39   Several national metrology institutes (NMIs) or designated institutes (DIs) provide

40   traceability by the use of high purity solid materials ($w_{pur} \geq 0.999$ g g^{-1}) with completely

41   known impurities (metals and non-metals), yielding a purity with an associated expanded

42   uncertainty of less than 0.01 %. In some cases, the distribution of selected impurities

43   among subsamples of the solid materials have been also investigated [1]. Based on these

44   solid materials, primary reference solutions with an expanded uncertainty associated with

45   the mass fraction of less than 0.05 % are gravimetrically prepared and metrologically

46   monitored by NMIs [2].

47   As the pure and fully characterized materials and the primary solutions have a limited

48   availability and are very valuable concerning the characterization and preparation

49   process, secondary solutions are prepared using pure materials usually only characterized

50   regarding metallic impurities. Therefore, these secondary solutions must be linked up to

51   the primary solutions. The expanded measurement uncertainty of the linkup must be less

52   than 0.1 % to achieve a calibration measurement of commercial solutions with an

53   expanded uncertainty associated with the mass fraction of 0.3 %. Overall, this procedure

54   demonstrates an unbroken chain of calibrations to link up the measurement results in the

55   field to the SI [3].

56   In this framework, high precision measurements are needed to link up the solutions with

57   a relative expanded uncertainty of less than 0.1 %. In most cases, those measurements are

58   being performed using the inductively coupled plasma optical emission spectrometry

59   (ICP OES) technique.

60   Given that the application of instrumental neutron activation analysis (INAA) technique

61   is missing in this field, a measurement procedure is suggested and the related

62   measurement model is obtained from the neutron activation equation. In addition, the

63   proposed procedure was experimentally tested in the case of two Mo solutions having the

64   same mass fraction, i.e. when the ratio is expected to be the unit value.

Measurement procedure and model

66   The aim of the measurement is to link up an elemental solution ES1 to an elemental

67   solution ES2 having mass fractions $w_{ES1}(E)$ and $w_{ES2}(E)$ of an element E by determining

68   the ratio

69
$$\tau = \frac{w_{ES1}(E)}{w_{ES2}(E)} \tag{1}$$

70   with a relative expanded uncertainty of 0.1 %.

71   To accomplish this aim, two measurement solutions, mS1 and mS2, are stocked in two

72   different containers by adding a sample (aliquot) of a monitor solution MS having a mass

73   fraction $w_{MS}(E_M)$ of a monitor element E_M to a sample of each elemental solution. Two

74   sub-samples of the measurement solutions, mS1,s and mS2,s, are used in the neutron

75   activation experiment.

76   To achieve the target uncertainty, attention has to be given to the evaporation of the

77   solution during handling. The elemental solution starts to evaporate with a mass rate α_{ES}

78   when it is transferred from its bottle to the container. After a time t_{MS}, the monitor

79   solution is pipetted into the container to obtain the final measurement solution. The

80   solution carries on evaporating during a time t_{mS}, with a mass rate α_{mS}, until a sub-sample

81   is taken and pipetted into an irradiation vial.

82   Hence, when the sub-samples are taken, the masses of the measurement solutions are

83    $m_{mS1} = m_{ES1} - \alpha_{E1}\,t_{MS1} + m_{1,MS} - \alpha_{mS1}\,t_{mS1}$ and $m_{mS2} = m_{ES2} - \alpha_{E2}\,t_{MS2} + m_{2,MS} - \alpha_{mS2}\,t_{mS2}$,

84   where m_{ES1}, m_{ES2} are the masses of the samples of ES1, ES2 and $m_{1,MS}$, $m_{2,MS}$ are the

85   additional masses of MS.

86   The mass fractions of E and E_M in the measurement solutions are

87
$$w_{\text{mS1}}(\text{E}) = \frac{w_{\text{ES1}}(\text{E})}{1 + \dfrac{m_{1,\text{MS}} - m_{\text{ev1}}}{m_{\text{ES1}}}}, \quad w_{\text{mS2}}(\text{E}) = \frac{w_{\text{ES2}}(\text{E})}{1 + \dfrac{m_{2,\text{MS}} - m_{\text{ev2}}}{m_{\text{ES2}}}} \tag{2}$$

88   and

89
$$w_{\text{mS1}}(\text{E}_\text{M}) = \frac{w_{\text{MS}}(\text{E}_\text{M})}{1 + \dfrac{m_{\text{ES1}} - m_{\text{ev1}}}{m_{1,\text{MS}}}}, \quad w_{\text{mS2}}(\text{E}_\text{M}) = \frac{w_{\text{MS}}(\text{E}_\text{M})}{1 + \dfrac{m_{\text{ES2}} - m_{\text{ev2}}}{m_{2,\text{MS}}}}, \tag{3}$$

90   respectively, where $m_{\text{ev1}} = \alpha_{\text{E1}} \, t_{\text{MS1}} + \alpha_{\text{mS1}} \, t_{\text{mS1}}$ and $m_{\text{ev2}} = \alpha_{\text{E2}} \, t_{\text{MS2}} + \alpha_{\text{mS2}} \, t_{\text{mS2}}$ are the

91   evaporated masses.

92   The number of atoms of an isotope ^iE of E and of an isotope $^i\text{E}_\text{M}$ of E_M in mS1,s and

93   mS2,s are

94
$$n_{\text{mS1,s}}(^i\text{E}) = \frac{x(^i\text{E}) \, N_\text{A} \, w_{\text{mS1}}(\text{E}) \, m_{\text{mS1,s}}}{M(\text{E})}, \quad n_{\text{mS2,s}}(^i\text{E}) = \frac{x(^i\text{E}) \, N_\text{A} \, w_{\text{mS2}}(\text{E}) \, m_{\text{mS2,s}}}{M(\text{E})}, \tag{4}$$

95   and

96
$$n_{\text{mS1,s}}(^i\text{E}_\text{M}) = \frac{x(^i\text{E}_\text{M}) \, N_\text{A} \, w_{\text{mS1}}(\text{E}_\text{M}) \, m_{\text{mS1,s}}}{M(\text{E}_\text{M})}, \quad n_{\text{mS2,s}}(^i\text{E}_\text{M}) = \frac{x(^i\text{E}_\text{M}) \, N_\text{A} \, w_{\text{mS2}}(\text{E}_\text{M}) \, m_{\text{mS2,s}}}{M(\text{E}_\text{M})}, \tag{5}$$

97   respectively, where $m_{\text{mS1,s}}$ and $m_{\text{mS2,s}}$ are the masses of mS1,s and mS2,s, N_A is the

98   Avogadro constant, $x(^i\text{E})$ and $x(^i\text{E}_\text{M})$ are the mole fractions of ^iE and $^i\text{E}_\text{M}$, $M(\text{E})$ and

99    $M(\text{E}_\text{M})$ are the molar masses of E and E_M, respectively. Here and hereafter the subscript

100   M refers to the monitor element.

101   From (1), (2) and (4) it follows

102
$$\tau = \frac{\left(1 + \dfrac{m_{1,\text{MS}} - m_{\text{ev1}}}{m_{\text{ES1}}}\right) \dfrac{n_{\text{mS1,s}}(^i\text{E})}{m_{\text{mS1,s}}}}{\left(1 + \dfrac{m_{2,\text{MS}} - m_{\text{ev2}}}{m_{\text{ES2}}}\right) \dfrac{n_{\text{mS2,s}}(^i\text{E})}{m_{\text{mS2,s}}}}. \tag{6}$$

103   The two sub-samples of the measurement solutions, mS1,s and mS2,s, are co-irradiated in

104   a neutron flux to activate the target isotopes ^{i}E and ^{i}E$_M$.

105   The counting of the γ-photons emitted during the radioactive decay of the radionuclide

106   produced by activation of the target isotope ^{i}E allows to quantify the ratio

107
$$\frac{n_{\mathrm{mS1,s}}(^i\mathrm{E})}{n_{\mathrm{mS2,s}}(^i\mathrm{E})}=\kappa_{\mathrm{td}}\ \kappa_{\mathrm{R}}\ \kappa_{\varepsilon}\ \kappa_{\mathrm{ss}}\ \kappa_{\mathrm{sa}}\ \kappa_{\mathrm{g}}\ \frac{C_{\mathrm{mS1,s}}(t_{\mathrm{d\ mS1,s}})}{C_{\mathrm{mS2,s}}(t_{\mathrm{d\ mS2,s}})}\ , \tag{7}$$

108   where $C(t_{\mathrm{d}})$ is the full-energy γ-peak detection count rate at a time t_{d} after the end of the

109   irradiation; here and hereafter, the subscripts mS1,s and mS2,s are occasionally omitted

110   in $C(t_{\mathrm{d}})$. The correction factors $\kappa_{\mathrm{td}}=e^{-\lambda(t_{\mathrm{d\ mS2,s}}-t_{\mathrm{d\ mS1,s}})}$, $\kappa_{\mathrm{R}}=R_{\mathrm{mS2,s}}/R_{\mathrm{mS1,s}}$,

111     $\kappa_{\varepsilon}=\varepsilon_{\mathrm{mS2,s}}/\varepsilon_{\mathrm{mS1,s}}$, $\kappa_{\mathrm{ss}}=k_{\mathrm{ss\ mS2,s}}/k_{\mathrm{ss\ mS1,s}}$, $\kappa_{\mathrm{sa}}=k_{\mathrm{sa\ mS2,s}}/k_{\mathrm{sa\ mS1,s}}$ and

112     $\kappa_{\mathrm{g}}=k_{\mathrm{g\ mS2,s}}/k_{\mathrm{g\ mS1,s}}$ take the differences of decay time, reaction rate, detection

113   efficiency, self-shielding, self-absorption and geometry of the sub-samples into account.

114   In detail, λ is the decay constant of the produced radionuclide, R is the reaction rate per

115   target isotope ^{i}E, ε is the detection full-energy γ efficiency for a point-like source located

116   at the center of mass of the sub-sample, k_{ss}, k_{sa}, and k_{g} are the neutron self-shielding, the

117   gamma self-absorption and the geometry factors, respectively.

118   It is worth to note that in the case of a radionuclide which emits γ-photons with several

119   energies E$_\gamma$, best results are achieved by using in (7) the mean value of the count rate

120   ratios, $\left.\dfrac{C_{\mathrm{mS1,s}}(t_{\mathrm{d\ mS1,s}})}{C_{\mathrm{mS2,s}}(t_{\mathrm{d\ mS2,s}})}\right|_{\mathrm{m}}$, obtained with different E$_\gamma$.

121   The γ-counting is carried out using germanium detectors. The count rate $C(t_{\mathrm{d}})$ is obtained

122   by averaging n values, $C_i(t_{\mathrm{d}})$, acquired in a γ-spectrometry sequence starting at a decay

123   time $t_{\mathrm{d\ 1}}$ after the end of the irradiation and consisting of n consecutive counts performed

124   during the decay of the produced radionuclide. More explicitly, each ith count rate value,

125     $C_i(t_{\mathrm{d}})$, extrapolated to t_{d} from the ith count of the sequence, starting at $t_{\mathrm{d\ }i}$ and lasting $t_{\mathrm{c\ }i}$, is

126
$$C_i(t_d) = \frac{\lambda\, n_{c\,i}}{e^{-\lambda\,(t_{d\,i}-t_d)}(1-e^{-\lambda\,t_{c\,i}})}\,\frac{t_{c\,i}}{t_{c\,i}-t_{dead\,i}}, \qquad (8)$$

127 where $n_{c\,i}$ and $t_{dead\,i}$ are the net count of the full-energy γ-peak and the detection dead time

128 of the ith count, respectively.

129 In the case of a $1/E^{1+\alpha}$ epithermal spectrum and if the target isotope ^iE is activated via a

130 (n,γ) reaction having a cross section with a $E^{-1/2}$ energy dependence, the reaction rate can

131 be described using the Høgdahl convention [4], $R = \Phi_{ep}\,\sigma_{0,E}\,(f + Q_{0,E}(\alpha))$, where Φ_{ep} is

132 the epithermal neutron flux, $f = \Phi_{th}/\Phi_{ep}$ is the thermal (sub-cadmium) to epithermal

133 neutron flux ratio, $\sigma_{0,E}$ is the (n,γ) cross section of ^iE at 0.0253 eV and

134
$$Q_{0,E}(\alpha) = (Q_{0,E} - 0.429)\overline{E}_r^{-\alpha} + \frac{0.429}{(2\alpha+1)\,0.55^{\alpha}}. \qquad (9)$$

135 In (9) $Q_{0,E}$ is the ratio between the resonance integral of ^iE for a $1/E$ epithermal spectrum,

136 $I_{0,E}$, and $\sigma_{0,E}$, and $\overline{E}_r$ is the effective resonance energy of ^iE [5].

137 Thus, the characteristics of the neutron energy spectrum affect the κ_R correction factor

138 according to

139
$$\kappa_R = \frac{\Phi_{ep2}(f_2 + Q_{0,E}(\alpha_2))}{\Phi_{ep1}(f_1 + Q_{0,E}(\alpha_1))}, \qquad (10)$$

140 where Φ_{ep1}, f_1, α_1 and Φ_{ep2}, f_2, α_2 are referred to the irradiation positions of mS1,s and

141 mS2,s, respectively.

142 Several methods have been developed and used to measure the neutron flux parameters;

143 as examples, (i) the "Cd-covered multi-monitor", the "Cd-ratio for multi-monitor" and

144 the "bare multi-monitor" methods for α, (ii) the "Cd-ratio" for Φ_{ep} and f, (iii) the "bare

145 bi-isotopic monitor" method for f [5]. These methods are usually applied offline, i.e.

146 before (or after) the experiment, by assuming that the neutron energy spectrum remains

147 constant and do not depend on the irradiation samples.

148   In our case, since the κ_R value is required with a relative expanded uncertainty of less

149   than 0.1 %, online information is valuable. To reach this aim, the monitor solution is

150   added to the elemental solution. If the Høgdahl convention applies to the target isotope

151    $^{i}E_M$,

152
$$\kappa_{\text{M-R}} = \frac{\Phi_{\text{ep2}}(f_2 + Q_{0,\text{EM}}(\alpha))}{\Phi_{\text{ep1}}(f_1 + Q_{0,\text{EM}}(\alpha))} . \tag{11}$$

153   From (10) and (11) it follows

154
$$\kappa_R = \kappa_{\text{M-R}} \frac{1 + \dfrac{\alpha_Q \, Q_{0,\text{E}}(\alpha)}{f_1 + Q_{0,\text{E}}(\alpha)}}{1 + \dfrac{\alpha_Q \, Q_{0,\text{E}}(\alpha)}{f_1(1 + \alpha_f) + Q_{0,\text{E}}(\alpha)}}, \tag{12}$$

155   where $\alpha_Q = \dfrac{Q_{0,\text{EM}}(\alpha) - Q_{0,\text{E}}(\alpha)}{Q_{0,\text{E}}(\alpha)}$ and $\alpha_f = \dfrac{f_2 - f_1}{f_1}$.

156   The counting of the γ-photons emitted during the radioactive decay of the radionuclide

157   produced by activation of the target isotope $^{i}E_M$ allows to determine

158
$$\kappa_{\text{M-R}} = (\kappa_{\text{M-td}} \, \kappa_{\text{M-}\varepsilon} \, \kappa_{\text{M-ss}} \, \kappa_{\text{M-sa}} \, \kappa_{\text{M-g}})^{-1} \frac{C_{\text{M-mS2,s}}(t_{\text{d M-mS2,s}})}{C_{\text{M-mS1,s}}(t_{\text{d M-mS1,s}})} \frac{n_{\text{mS1,s}}(^{i}E_M)}{n_{\text{mS2,s}}(^{i}E_M)} . \tag{13}$$

159   According to (3) and (5), the ratio

160
$$\frac{n_{\text{mS1,s}}(^{i}E_M)}{n_{\text{mS2,s}}(^{i}E_M)} = \frac{m_{\text{mS1,s}}\left(1 + \dfrac{m_{\text{ES2}} - m_{\text{ev2}}}{m_{2,\text{MS}}}\right)}{m_{\text{mS2,s}}\left(1 + \dfrac{m_{\text{ES1}} - m_{\text{ev1}}}{m_{1,\text{MS}}}\right)} . \tag{14}$$

161   In conclusion, the measurement model adopted to link up ES1 to ES2 is obtained from

162   (6), (7), (12), (13) and (14):

163

$$\tau = \frac{m_{ES2}}{m_{ES1}} \frac{m_{1,MS}}{m_{2,MS}} \frac{C_{mS1,s}(t_{d\,mS1,s})}{C_{mS2,s}(t_{d\,mS2,s})} \frac{C_{M-mS2,s}(t_{d\,M-mS2,s})}{C_{M-mS1,s}(t_{d\,M-mS1,s})}$$
$$\times \beta_R \, \kappa_{td} \, \kappa_{M-td}^{-1} \, \kappa_{ss} \kappa_{M-ss}^{-1} \, \kappa_{sa} \kappa_{M-sa}^{-1} \, \kappa_{g} \kappa_{M-g}^{-1} \, \kappa_{\varepsilon} \kappa_{M-\varepsilon}^{-1}$$

(15)

164 where $\beta_R = \dfrac{1 + \dfrac{\alpha_Q \, Q_{0,E}(\alpha)}{f_1 + Q_{0,E}(\alpha)}}{1 + \dfrac{\alpha_Q \, Q_{0,E}(\alpha)}{f_1(1+\alpha_f) + Q_{0,E}(\alpha)}}$.

165 It is remarkable that the result is independent on the masses of the evaporated solutions

166 m_{ev1}, m_{ev2}, on the masses of the irradiated sub-samples $m_{mS1,s}$, $m_{mS2,s}$ and on the

167 epithermal flux at the irradiation positions Φ_{ep1}, Φ_{ep2}. Moreover, in case of (i) large f, (ii)

168 $Q_{0,EM}(\alpha) \cong Q_{0,E}(\alpha)$ or (iii) $f_1 \cong f_2$, the result becomes less affected by the f, α, $\overline{E}_r$, $Q_{0,E}$,

169 and $Q_{0,EM}$ values.

170 **Experimental**

171 The proposed procedure was tested using a Mo solution having a mass fraction

172 $w(Mo) \approx 1$ g kg^{-1}. In this preliminary experiment, a Co solution having a mass fraction

173 $w(Co) \approx 1$ g kg^{-1} was adopted as the monitor solution. The Mo and Co solutions were

174 obtained using ultrapure ammonium molybdate tetrahydrate, $(NH_4)_6Mo_7O_{24} \cdot 4\,H_2O$, in

175 water and ultrapure Co metal in 0.5 mol L^{-1} nitric acid, respectively.

176 A single measurement solution, mS, was prepared in a container by adding the Co

177 solution to the Mo solution. Two sub-samples were taken and used for the neutron

178 irradiation. This mimics the application of the procedure in the case of two Mo solutions

179 having the same mass fraction, i.e. $w_{ES1}(E) = w_{ES2}(E)$, $m_{ES1} = m_{ES2}$, $m_{1,MS} = m_{2,MS}$. To

180 attain the objective, (15) must be satisfied, i.e. $\tau = 1$, with a relative expanded

181 uncertainty of 0.1 %.

182 The τ value was determined by counting (i) the 140.51 keV γ-photons emitted during the

183 radioactive decay of ^{99}Mo and ^{99m}Tc in equilibrium conditions and produced by

184   activation of ^{98}Mo via the (n,γ) neutron capture reaction, and (ii) the 1173.23 keV and

185   1332.49 keV γ-photons emitted during the radioactive decay of ^{60}Co produced by

186   activation of ^{59}Co via the (n,γ) neutron capture reaction.
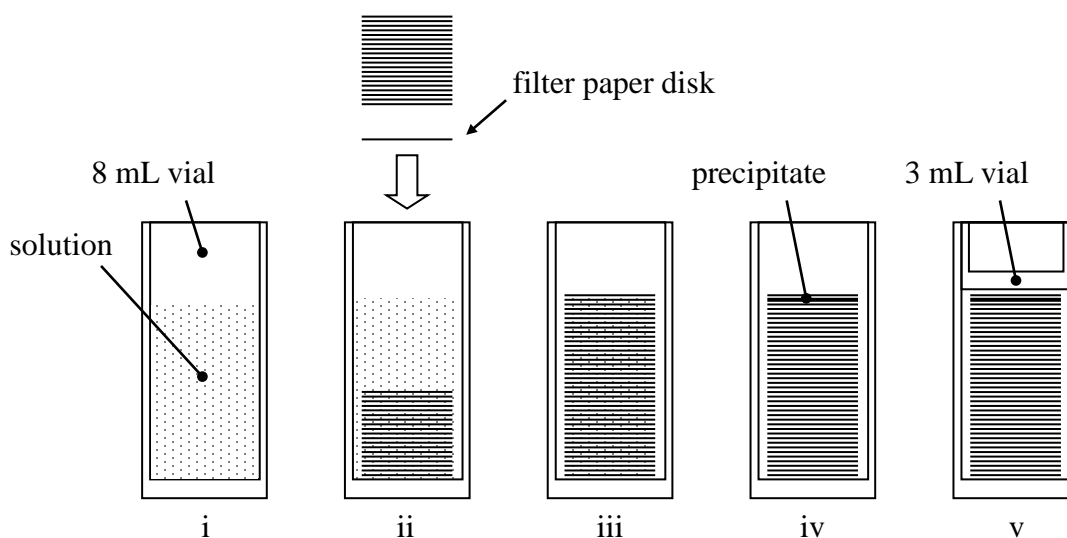
Preparation of the measurement solution

188   The measurement solution was prepared by pipetting the Co solution to a 25 mL

189   polytetrafluoroethylene (PTFE) flask filled with the Mo solution. To correct for the effect

190   of the evaporation, the mass of the measurement solution, m_{mS}, was recorded

191   continuously during its preparation with a sampling frequency of 1 Hz. The data were

192   collected using a digital analytical balance having a resolution of 0.01 mg and calibrated

193   with SI-traceable weights. It is noteworthy that, although the buoyancy affects the

194   weighing of the solution, the ratios of the masses in the model (15) eliminates the effect

195   on τ. Therefore, the weighed masses were not corrected for buoyancy.

196   The room temperature during the preparation was 26 °C. After setting to zero (tare) the

197   reading of the balance with the empty flask, (i) 21 mL of Mo solution, (ii) 125 μL of Co

198   solution and (iii) 6 mL of Mo solution were consecutively added at 179 s, 532 s and

199   993 s, respectively. The balance drift during the recording session was −0.02 mg.

200   A straight line was fitted to the data collected between (i) 223 s and 524 s, (ii) 623 s and

201   919 s, (iii) 1025 s and 1285 s. The evaporation rates were found to be 2.1×10^{-6} g s^{-1},

202   2.0×10^{-6} g s^{-1} and 3.3×10^{-6} g s^{-1}. According to the fitted data, the masses of the added

203   solutions at steps (i), (ii) and (iii) were $m_{ES} = 20.96218(4)$ g, $m_{MS} = 0.12572(4)$ g and

204    $m_{ES} = 6.07041(4)$ g, respectively. Here and hereafter, unless otherwise specified, the

205   brackets refer to the standard uncertainty. The residuals of the fitted data were on average

206   within ± 0.02 mg. However, since there are also spikes up to 0.04 mg, an uncertainty of

207   0.04 mg was assigned to the measured masses.

Preparation of the irradiation samples

209   Two sub-samples, 2 mL volumes, of the measurement solution, hereafter called samples,

210   were taken and pipetted in two different 8 mL polyethylene (PE) vials. Afterwards,

211   80 filter paper disks (12 mm diameter) obtained from a single sheet using a cutting punch

212   were inserted in both the PE vials. The paper disks were subsequently dried using an IR

213   lamp and pressed using a slice of a 3 mL vial sealed to the 8 mL vial. It was assumed that

214   the Mo and Co content of the pipetted solutions precipitates completely in the paper

215   disks; this was confirmed by subsequent measurements with the emptied PE vials. The

216   preparation of a sample for irradiation is summarized in Fig. 1.

217

218   **Fig. 1** Preparation of an irradiation sample; (i) the pipetted sub-sample of the
219   measurement solution, (ii) and (iii) insertion of the filter paper disks, (iv) paper disks
220   after drying, (v) sealed PE vial

221   The visual inspection of the PE vials after drying was evidence for a precipitation largely

222   occurring in the upper part of the piled disks (see the picture in Fig. S1). This was proof

223   that the Mo and Co solutes were not homogeneously distributed in the paper disks. Since

224   the mass fraction of the Co solution in the measurement solution was at 10^{-3} level, the

225   pipetted 2 mL solution consisted of 2 mg of Mo and the observed precipitate could have

226   been ammonium molybdate tetrahydrate.

227   To limit the effect of external contaminations, the PE vials, the tweezers used to handle

228   the filter paper disks were cleaned in an ultrasonic bath with diluted HNO_3 and the

229   cutting punch was washed with isopropyl alcohol. The water was purified using a

230   Millipore system ($\rho \geq 18$ MΩ). Concerning the filter paper, a previous neutron activation

231   experiment carried out with the disks did not show any contamination of Co and Mo.

232   *Neutron irradiation and gamma spectrometry*

233   The neutron irradiation lasted 3 h and was performed in the central channel of the

234   250 kW TRIGA Mark II reactor at the Laboratory of Applied Nuclear Energy (LENA) of

235   the University of Pavia. The nominal thermal and epithermal neutron fluxes were about

236   6×10^{12} cm^{-2} s^{-1} and 5.5×10^{11} cm^{-2} s^{-1}, resulting in a nominal f value of 10.9. The

237   samples were put in a PE container used for irradiation. Fig. 2 shows the position of the

238   container and the samples with respect to the equator of the reactor core.
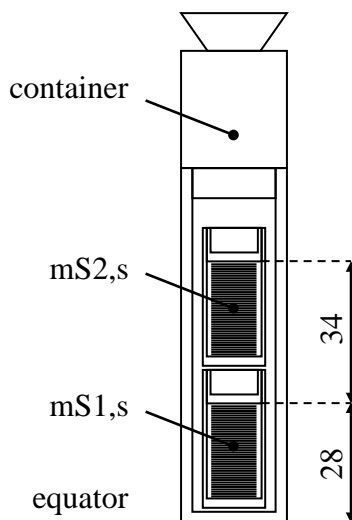
239

240   **Fig. 2** Position of the irradiation container and the samples with respect to the equator of
241   the reactor core; dimensions are in mm

242   After the neutron irradiation, the samples were extracted from the container, rinsed with

243   diluted HNO$_3$ and fixed to a γ-counting container (Fig. 3).

244
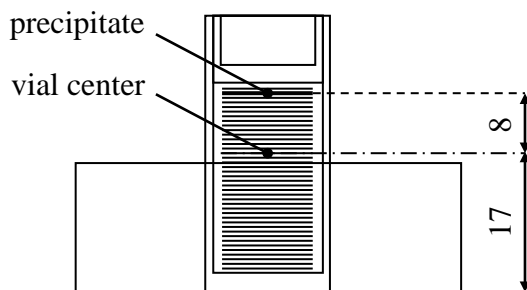
245 **Fig. 3** Position of the sample with respect to the γ-counting containers; dimensions are in
246 mm

247 The γ-detection was carried out using a detector Canberra GC3518 (relative efficiency

248 35 %, 1.80 keV FWHM resolution at 1332 keV), and a detector ORTEC$^{®}$ GEM50P4-83

249 (66 mm crystal diameter, 50 % relative efficiency, 1.90 keV FWHM resolution at

250 1332 keV).

251 Six γ-spectrometry sequences were recorded with a digital signal processor

252 ORTEC$^{®}$ DSPEC 502 and a personal computer running the software for data acquisition

253 ORTEC$^{®}$ Gamma Vision [6]. The first four sequences were performed with the GC3518

254 and concerned the 140.51 keV γ-emission of ^{99}Mo and ^{99m}Tc in equilibrium conditions.

255 The latter two γ-spectrometry sequences were performed with the GEM50P4-83 and

256 concerned the 1173.23 keV and 1332.49 keV γ-emission of ^{60}Co. Each sequence

257 consisted of n counts performed by adjusting on-line the counting window to reach a

258 0.23 % counting uncertainty. The dead to counting time ratio, t_{dead} / t_c, of the detection

259 systems during the data collection was always below 2.5 %. The position of the γ-

260 counting containers with respect to the detector during the first four and the latter two

261 sequences are displayed in Fig. 4a and Fig. 4b, respectively. In particular, the distances

262 between the bottom of the γ-counting container and the end-cap of the detector were

263 $d_{GC3518} = 230$ mm and $d_{GEM50P4-83} = 85$ mm.
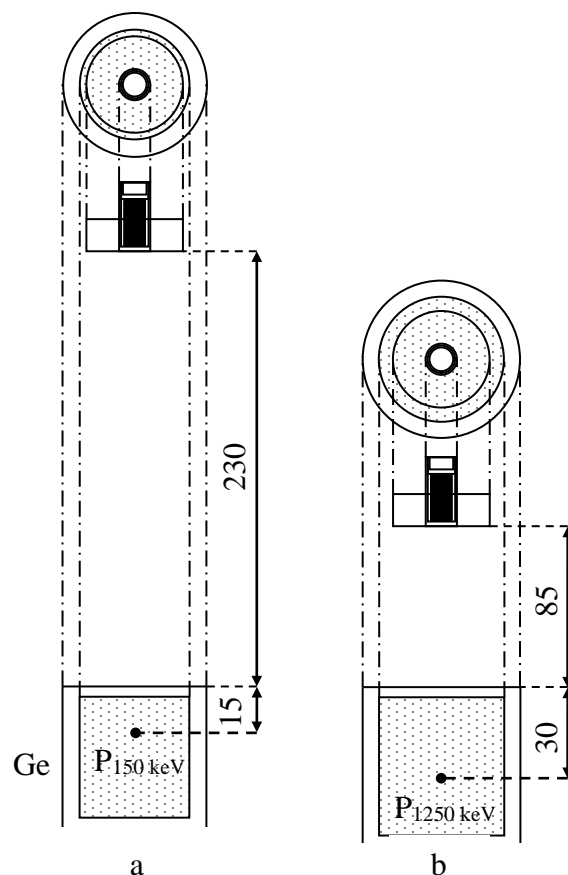
264
265 **Fig. 4** Position of the γ-counting containers (a) with respect to the detector GC3518
266 during ^{99}Mo and ^{99m}Tc detection and (b) with respect to the detector GEM50P4-83 during
267 the ^{60}Co detection. The point $P_{E\gamma}$ defines the (virtual) vertical position within the Ge
268 crystal where the detection efficiency ε tends to infinite; dimensions are in mm

269 The sequence number, the sample, the decay time at the beginning of the sequence, $t_{d\,1}$,
270 and the number of collected counts, n, are summarized in table 1. The first sequence
271 started about 4 days after the end of the irradiation to assure a negligible effect due to the
272 ^{99}Mo and ^{99m}Tc equilibrium conditions [5].

273 **Table 1** The sample, the decay time, $t_{d\,1}$, and the number of collected counts, n, in each
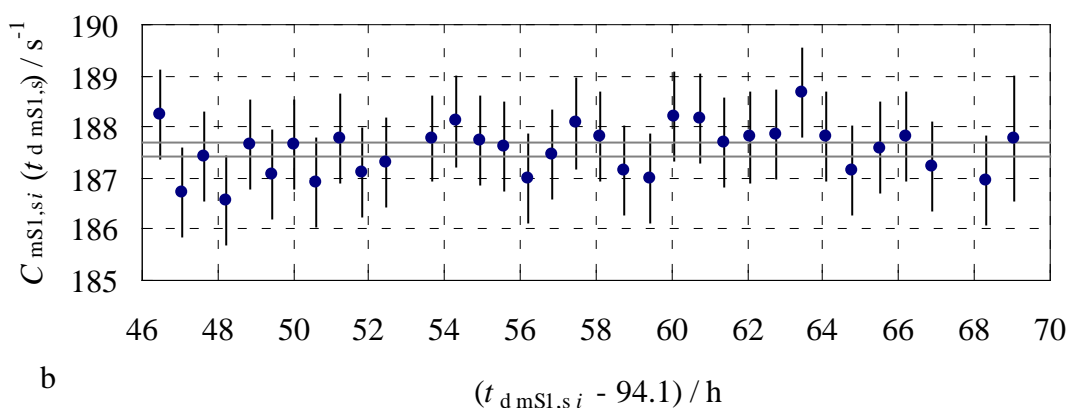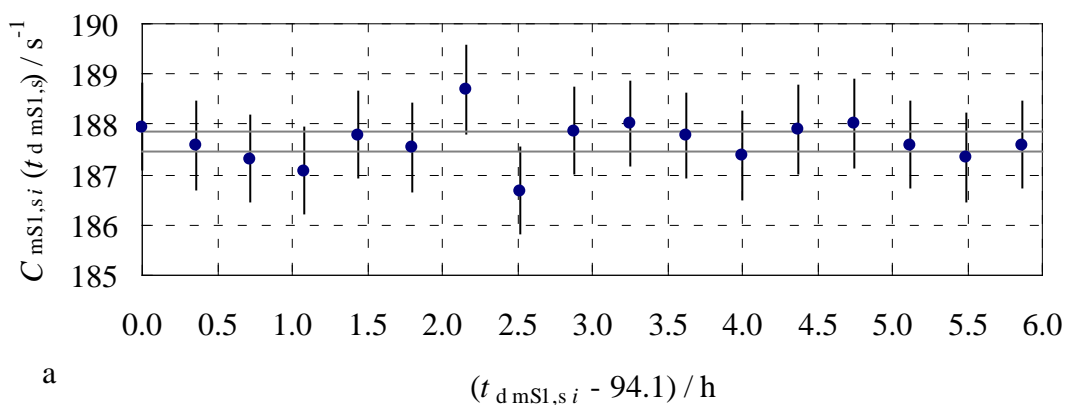274 sequence

sequence	sample	$t_{d\,1}$ / h	counts / n
1	mS1,s	94.1	17
2	mS2,s	118.3	38
3	mS1,s	152.9	36
4	mS2,s	163.6	27

| 5 | mS1,s | 692 | 14 |
| 6 | mS2,s | 1058 | 22 |

Results and discussion

276 The count rate of the ith count of the sequence, $C_i(t_d)$, was computed according to (8). The

277 decay constants, $\lambda = \ln(2) / t_{1/2}$, were calculated using the half-life literature values, i.e.

278 $t_{1/2}(^{99}\text{Mo}, {}^{99m}\text{Tc}) = 65.976(24)\,\text{h}$ (in equilibrium conditions) and

279 $t_{1/2}(^{60}\text{Co}) = 1925.28(14)\,\text{d}$ [7, 8]. The net count, $n_{c\,i}$, was obtained by fitting the full-

280 energy γ-peak with the algorithm implemented on the Gamma Vision software (analysis

281 engine wan32 G53W2.06).

282 The 140.51 keV $^{99}\text{Mo}, {}^{99m}\text{Tc}$ count rates, extrapolated to $t_{d\,mS1,s} = 94.1\,\text{h}$ and

283 $t_{d\,mS2,s} = 118.3\,\text{h}$, are reported in Fig. 5. Here and hereafter, the error bars indicate the

284 95 % confidence interval due to counting statistics.

a

b

c

d
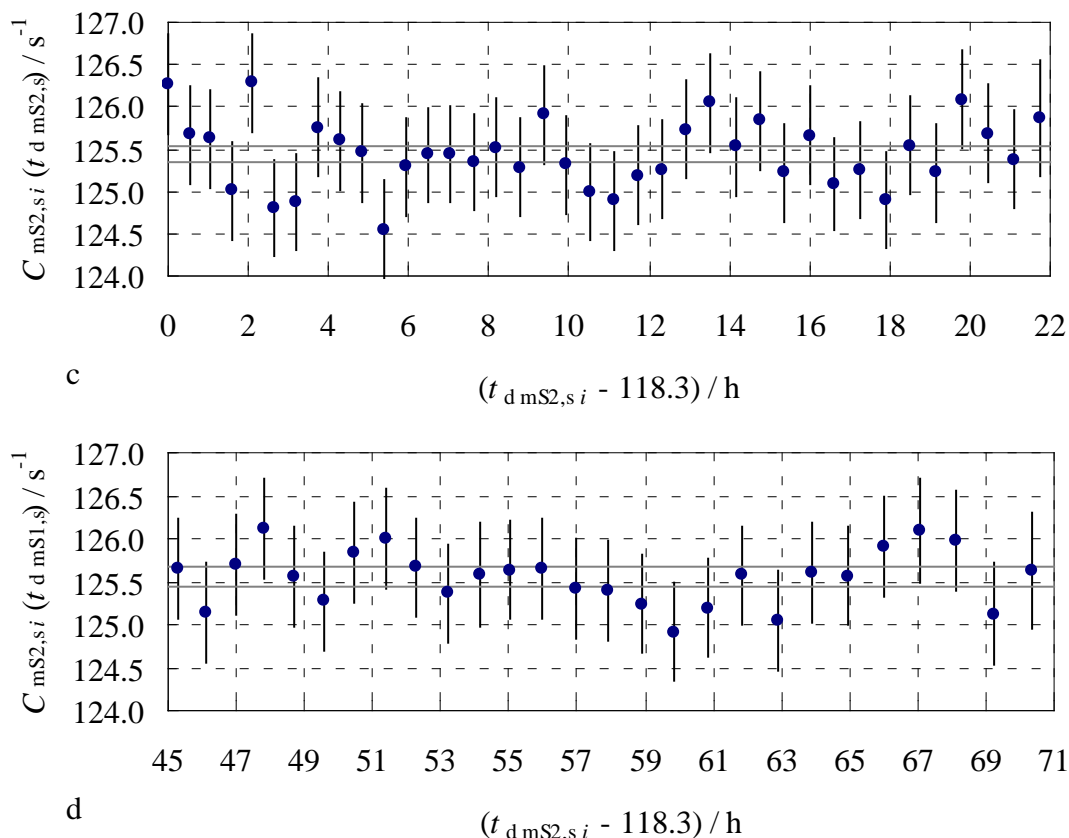
Fig. 5 The 140.51 keV ^{99}Mo, ^{99m}Tc count rates of the mS1,s sample extrapolated to $t_{d\,mS1,s} = 94.1$ h and recorded during (a) the sequence 1 and (b) the sequence 3. The 140.51 keV ^{99}Mo, ^{99m}Tc count rates of the mS2,s sample extrapolated to $t_{d\,mS2,s} = 118.3$ h and recorded during (c) the sequence 2 and (d) the sequence 4. The horizontal lines show the 95 % confidence interval associated to the mean of the count rate values

The mean values of the 140.51 keV ^{99}Mo, ^{99m}Tc count rates recorded with the mS1,s and the mS2,s samples, extrapolated to $t_{d\,mS1,s} = 94.1$ h and $t_{d\,mS2,s} = 118.3$ h, were $C_{mS1,s}(t_{d\,mS1,s}) = 187.589(61)$ s^{-1} and $C_{mS2,s}(t_{d\,mS2,s}) = 125.486(36)$ s^{-1}, respectively (uncertainties are due to counting statistics). The horizontal lines in Fig. 5 show the 95 % confidence interval associated to the mean of the count rates values. The count rate ratio,

$\dfrac{C_{mS1,s}(t_{d\,mS1,s})}{C_{mS2,s}(t_{d\,mS2,s})}$, was 1.49490(65) s^{-1}.

The 1173.23 keV and 1332.49 keV ^{60}Co count rates are reported in Fig. 6.

16

a

b

c
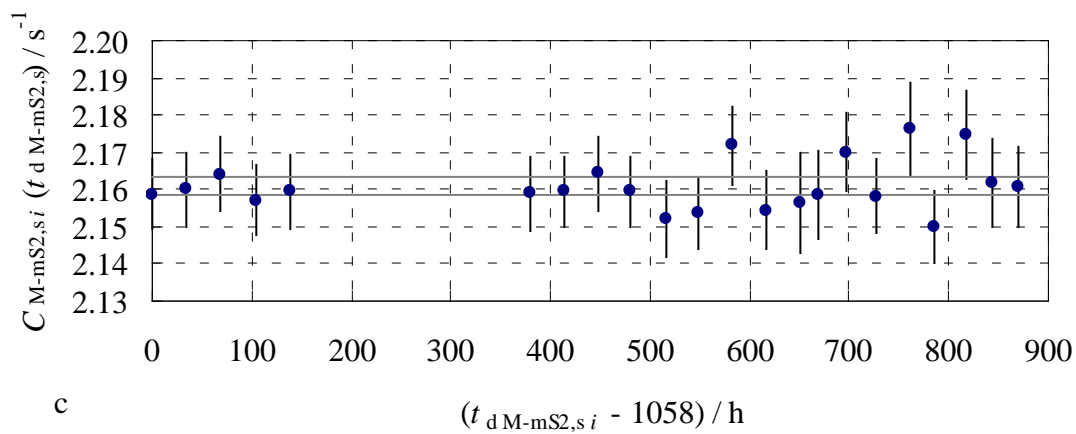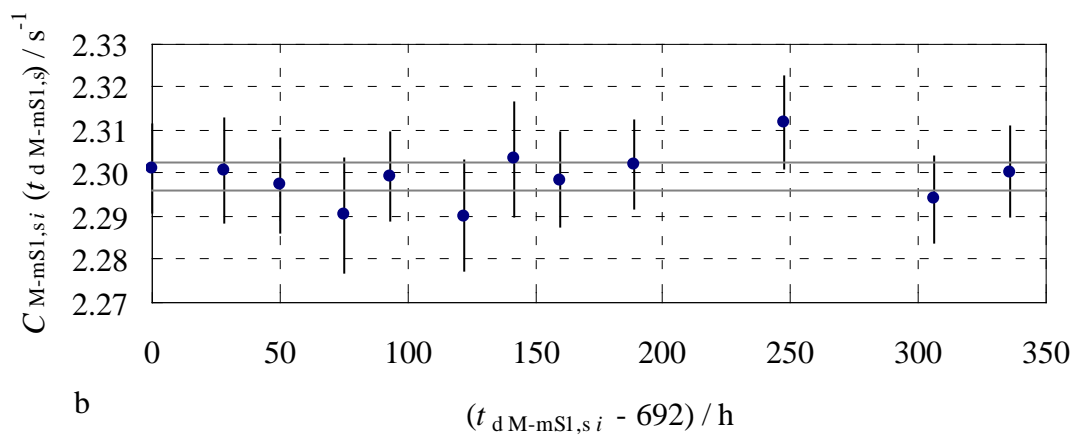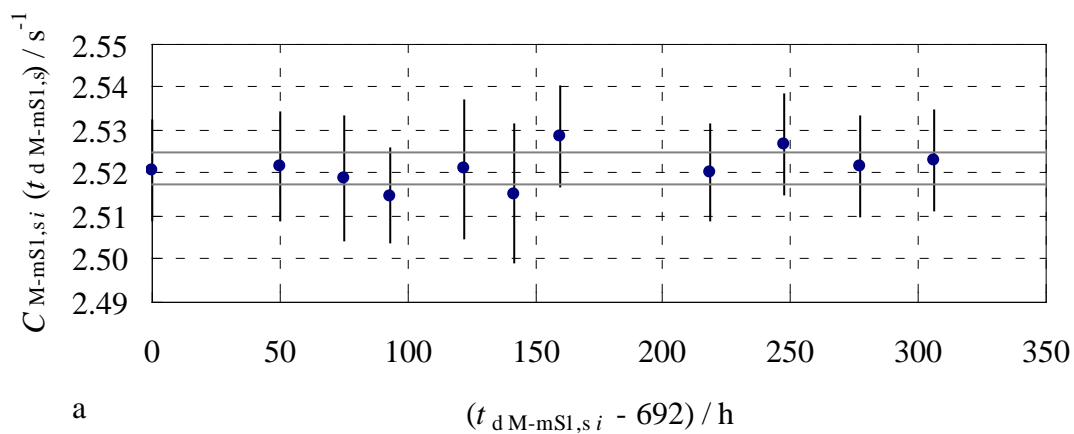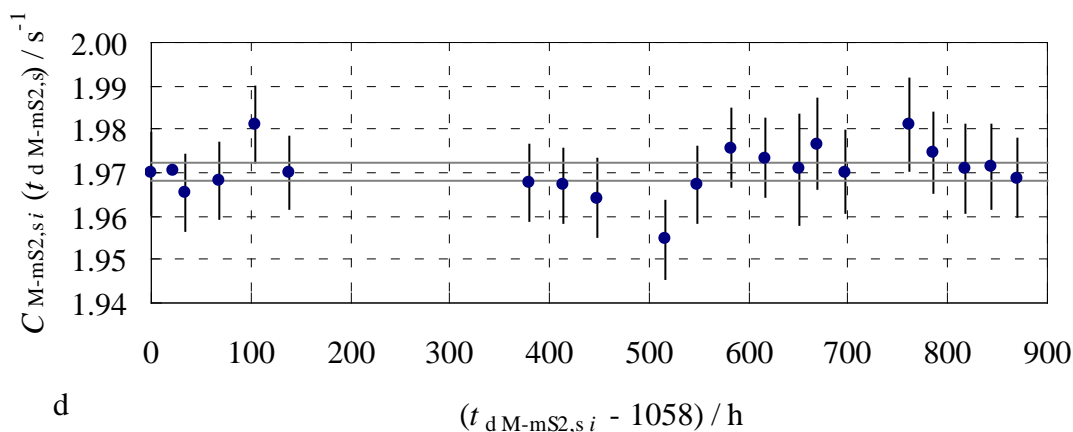
Fig. 6 (a) The 1173.23 keV and (b) the 1332.49 keV ^{60}Co count rates of the mS1,s sample recorded during the sequence 5 and extrapolated to $t_{\text{d M-mS1,s}} = 692$ h. (c) The 1173.23 keV and (d) the 1332.49 keV ^{60}Co count rates of the mS2,s sample recorded during the sequence 6 and extrapolated to $t_{\text{d M-mS2,s}} = 1058$ h. The horizontal lines show the 95 % confidence interval associated to the mean of the count rate values

The mean values of the 1173.23 keV ^{60}Co count rates recorded with the mS1,s and the mS2,s samples, extrapolated to $t_{\text{d M-mS1,s}} = 692$ h and $t_{\text{d M-mS2,s}} = 1058$ h, were $C_{\text{M-mS1,s}}(t_{\text{d M-mS1,s}}) = 2.5212(19)$ s^{-1} and $C_{\text{M-mS2,s}}(t_{\text{d M-mS2,s}}) = 2.1609(11)$ s^{-1}, respectively; the mean values of the 1332.49 keV ^{60}Co count rates recorded with the mS1,s and the mS2,s samples, extrapolated to $t_{\text{d M-mS1,s}} = 692$ h and $t_{\text{d M-mS2,s}} = 1058$ h, were $C_{\text{M-mS1,s}}(t_{\text{d M-mS1,s}}) = 2.2991(16)$ s^{-1} and $C_{\text{M-mS2,s}}(t_{\text{d M-mS2,s}}) = 1.9704(10)$ s^{-1}, respectively (uncertainties are due to counting statistics). The horizontal lines in Fig. 6 show the 95 % confidence interval associated to the mean of the ^{60}Co count rates values. The weighted mean value of the count rate ratios, $\left. \dfrac{C_{\text{M-mS2,s}}(t_{\text{d M-mS2,s}})}{C_{\text{M-mS1,s}}(t_{\text{d M-mS1,s}})} \right|_{\text{m}}$, was 0.85708(55) s^{-1}.

Correction Factors

The differences $t_{\text{d mS2,s}} - t_{\text{d mS1,s}}$ and $t_{\text{d M-mS2,s}} - t_{\text{d M-mS1,s}}$ were 24.2 h and 366 h, respectively, i.e. about 0.4 times $t_{1/2}(^{99}\text{Mo}, {}^{99\text{m}}\text{Tc})$ and 8×10^{-3} times $t_{1/2}(^{60}\text{Co})$. Accordingly, $\kappa_{\text{td}} = 0.77554$ and $\kappa_{\text{M-td}} = 0.99452$ with negligible uncertainties.

315   The measurement solutions had a similar Mo and Co mass fraction and the pipetted

316   subsamples had the same volume. In the case of a 1 mm thick, 12 mm diameter sample

317   with 2 mg Mo and 10 μg Co, the neutron self-shielding factor is 0.998 for Mo and 1.000

318   for Co, i.e. 0.2 % epithermal neutron self-shielding for Mo. Even if the solutes were not

319   uniformly distributed in the paper disks, the neutron self-shielding factors

320    $k_{ss\ mS1,s} = k_{ss\ mS2,s}$, $k_{M\text{-}ss\ mS1,s} = k_{M\text{-}ss\ mS2,s}$.   Similarly,   the γ-self-absorption   factors

321    $k_{sa\ mS1,s} = k_{sa\ mS2,s}$, $k_{M\text{-}sa\ mS1,s} = k_{M\text{-}sa\ mS2,s}$ and   the   geometry   factors $k_{g\ mS1,s} = k_{g\ mS2,s}$,

322    $k_{M\text{-}g\ mS1,s} = k_{M\text{-}g\ mS2,s}$. Thus, $\kappa_{ss} = \kappa_{M\text{-}ss}^{-1} = \kappa_{sa} = \kappa_{M\text{-}sa}^{-1} = \kappa_{g} = \kappa_{M\text{-}g}^{-1} = 1$ with negligible

323   uncertainty.

324   The full-energy γ-peak detection efficiency ε tends to infinite in a (virtual) vertical

325   position within the Ge crystal of the detector [9]. This position depends on the γ-photon

326   energy, E_γ, and is defined by a point, $P_{E\gamma}$ (see Fig. 4). A previous characterization of the

327   detectors showed that the distance between the end-cap and $P_{E\gamma}$ is $d_{150\ keV} = 15$ mm for

328   the GC3518 and $d_{1250\ keV} = 30$ mm for the GEM50P4-83. The distance betwen the center

329   of the PE vial and the bottom of the γ-counting container, d_c, and the distance between

330   the center of the PE vial and the precipitate, d_p, were 17 mm and 8 mm, respectively (see

331   Fig. 3). The detection efficiency correction factors are

332
$$\kappa_\varepsilon = \frac{(d_{Mo} + \Delta d_{Mo2})^2}{(d_{Mo} + \Delta d_{Mo1})^2} \text{ and } \kappa_{M\text{-}\varepsilon} = \frac{(d_{Co} + \Delta d_{Co2})^2}{(d_{Co} + \Delta d_{Co1})^2}, \tag{16}$$

333   where Δd_{Mo1} and Δd_{Mo2} are the distances between the Mo center of mass and the center

334   of the PE vial in sample 1 and 2, Δd_{Co1} and Δd_{Co2} are the distances between the

335   Co center of mass and the center of the PE vial in sample 1 and 2,

336    $d_{Mo} = d_{150keV} + d_{GC3518} + d_c = 262$ mm   and $d_{Co} = d_{1250keV} + d_{GEM50P4\text{-}83} + d_c = 132$ mm.

337   As examples, if in both the samples all the Mo and Co were in the precipitate, i.e.

338    $\Delta d_{Mo1} = \Delta d_{Mo2} = \Delta d_{Co1} = \Delta d_{Co2} = d_p$, $\kappa_\varepsilon = \kappa_{M\text{-}\varepsilon}^{-1} = 1$. Instead, if in sample 2 only a

339   fraction of Mo and Co was in the precipitate, i.e. $\Delta d_{Mo1} = \Delta d_{Co1} = d_p$ and

340    $\Delta d_{Mo2} = \Delta d_{Co2} = d_p - \Delta d_p$, in the case of $\Delta d_p = 4$ mm, $\kappa_\varepsilon = 0.985$ and $\kappa_{M\text{-}\varepsilon} = 0.971$.

341 Since the actual positions of Mo and Co centers of mass were not measured,

342 $\Delta d_p = \pm 4$ mm (uniform distribution) was preliminary assigned. Accordingly,

343 $\kappa_\varepsilon = 1.000(9)$ and $\kappa_{M\text{-}\varepsilon} = 1.000(16)$.

344 The literature Q_0 values for ^{98}Mo and ^{59}Co are 53.1(33) and 1.993(60) [10]. Experimental

345 data for the α value at the LENA irradiation channel are missing. However, based on the

346 $\alpha = $ -0.051(8) value at the central channel of the TRIGA Mark II reactor operating in

347 Ljubljana [11], from (9) it follows that $Q_{0,Mo}(\alpha) = 70(9)$, $Q_{0,Co}(-0.051) = 2.5(6)$ and

348 $\alpha_Q = $ -0.965(10).

349 Due to the 10.9 nominal f value, about 85% of the ^{60}Co activity was produced by thermal

350 neutrons. As the ^{60}Co count rate of sample 2 to the count rate of sample 1 ratio was about

351 0.86, the Φ_{th1} was approximately 16 % higher than Φ_{th2} and a possible variation of f could

352 be expected. In the case of $\alpha_f = \pm0.025$ (uniform distribution) and 10 % relative

353 uncertainty for the f value, $\beta_R = 1.000(10)$.

354 *Uncertainty budget*

355 The application of (15) to the experimental data collected in this study gave a ratio

356 $\tau = 0.999(19)$. The provisional uncertainty budget calculated according to the Guide to

357 the Expression of Uncertainty in Measurement [12] is reported in table 2.

358 **Table 2** Uncertainty budget of the measured ratio τ. The input quantities x_i are given in
359 the text. The index column gives the relative contributions of $u(x_i)$ to the combined
360 standard uncertainty, $u_c(y)$, of τ

Quantity	Unit	Value	Standard uncertainty	Index
X_i	$[X_i]$	x_i	$u(x_i)$	%
$m_{1,MS}$	g	0.12572	0.00004	0.0
$m_{2,MS}$	g	0.12572	0.00004	0.0
m_{ES1}	g	27.03259	0.00006	0.0

m_{ES2}	g	27.03259	0.00006	0.0
$C_{mS1,s}/C_{mS2,s}$	1	1.49490	0.00065	0.0
$C_{M\text{-}mS2,s}/C_{M\text{-}mS1,s}$	1	0.85708	0.00055	0.1
β_R	1	1.000	0.010	22.8
κ_{td}	1	0.77554	0.00000	0.0
$\kappa_{M\text{-}td}$	1	0.99452	0.00000	0.0
$\kappa_{ss}\,(\kappa_{M\text{-}ss})^{-1}$	1	1.00000	0.00000	0.0
$\kappa_{sa}\,(\kappa_{M\text{-}sa})^{-1}$	1	1.00000	0.00000	0.0
$\kappa_{g}\,(\kappa_{M\text{-}g})^{-1}$	1	1.00000	0.00000	0.0
κ_{ε}	1	1.000	0.009	18.5
$\kappa_{M\text{-}\varepsilon}$	1	1.000	0.016	58.5
Y	$[Y]$	y	$u_c(y)$	
τ	1	0.999	0.019	100.0

361   Given that the variation of the shape of the neutron energy spectrum and the detection
362   efficiency were the main influence factors, the following ways are suggested to reduce
363   their effects.

364   In particular, the measurement model shows that the adoption of a monitor element
365   having a Q_0 value similar to the Q_0 value of ^{99}Mo makes the result almost independent on
366   f, α, $Q_{0,E}$, and $Q_{0,EM}$ values. The best choice among the potential target elements is the
367   ^{116}Sn, which is neutron activated to ^{117}Sn via (n,γ) capture reaction and detected via the
368   158.56 keV γ-photons emitted during the radioactive decay of ^{117}Sn ($t_{1/2} = 13.76(4)$ d
369   [13]). The outcome of the $Q_0 = 56.3(11)$ value [10] of ^{116}Sn might be a $\beta_R = 1$ with a
370   relative uncertainty below 0.01 %.

371   Moreover, the actual position of the radionuclide center of mass with respect to the center
372   of the 8 mL PE vial can be experimentally determined by counting the sample right-side-
373   up and up-side-down. See equation (S1) in the supplementary information for detail.
374   Hence, the knowledge of the Δd_p value and the increase of the distance of the samples

375   from the detector during the γ-counting might limit the κ_ε and $\kappa_{M\text{-}\varepsilon}$ relative uncertainty

376   below 0.1 %.

377   **Conclusions**

378   The possibility of using the INAA technique to determine the ratio of the mass fractions

379   of two mono-elemental solutions with a relative expanded uncertainty of less than 0.1 %

380   was investigated. To reach the target uncertainty, the addition of a monitor solution to the

381   elemental solution was essential to correct for possible variation of the neutron energy

382   spectrum at the irradiation positions. A procedure was developed and the related

383   measurement model was obtained from the neutron activation equation.

384   The proposed measurement procedure was applied in a feasibility test in the case of two

385   Mo solutions having the same mass fraction, i.e. obtained from the same solution, and

386   using Co as the monitor element. The departure of the measured ratio from the unit value

387   (-0.1 %) was in agreement with the evaluated 1.9 % relative uncertainty. The uncertainty

388   budget pointed out that the main contributors were the variation of the shape of the

389   neutron energy spectrum and the detection efficiency.

390   The target 0.1 % relative expanded uncertainty was not achieved. Nevertheless, the use of

391   INAA to link up Mo solutions to the SI is promising; a considerable decrease of the

392   measurement uncertainty might be reached by improved sample preparation and an

393   improved γ-counting technique.

394   **Acknowledgements**

References

401

402 1. D'Agostino G, Bergamaschi L, Giordani L, Oddone M, Kipphardt H, Richter S (2014)
403   Use of Instrumental Neutron Activation Analysis to investigate the distribution of
404   trace elements among subsamples of solid materials. Metrologia 51:48-53

405 2. Kaltenbach A, Noordmann J, Görlitz V, Pape C, Richter S, Kipphardt H, Kopp G,
406   Jährling R, Rienitz O, Güttler B (2015) Gravimetric preparation and characterization
407   of primary reference solutions of molybdenum and rhodium. Anal Bioanal Chem
408   407:3093-3102

409 3. Rienitz O, Schiel D, Görlitz V, Jährling R, Vogl J, Lara-Manzano J V, Zoń A, Fung W
410   H, Buzoianu M, Caciano de Sena R, Augusto dos Reis L, Valiente L, Yim Y H, Hill S,
411   Champion R, Fisicaro P, Bing W, Turk G C, Winchester M R, Saxby D, Merrick J,
412   Hioki A, Miura T, Suzuki T, Linsky M, Barzev A, Máriássy M, Cankur O, Ari B,
413   Tunç M, Konopelko L A, Kustikov Y A, Bezruchko M (2012) Final report on CCQM-
414   K87: Mono-elemental calibration solutions. Metrologia DOI 10.1088/0026-
415   1394/49/1A/08010

416 4. Høgdahl OT (1965) Proceedings of the Symposium on Radiochemical Methods of
417   Analysis 1:23-40

418 5. De Corte F (1987) The k0-Standardisation Method. A move to the optimization of
419   Neutron Activation Analysis. Ed. Ryksuniversiteit Gent Faculteit Van de
420   Wettenschappen

421 6. GammaVision (2006) Version 6.08; Advanced Measurement Technology, Inc.:
422   Berwyn, PA

423 7. Browne E, Tuli J K (2011) Nucl Data Sheets 112:275-446

424 8. Browne E, Tuli J K (2013) Nucl Data Sheets 114:1849-2022

425 9. Gilmore G, Hemingway J D (1995) Practical Gamma-ray Spectrometry, New York,
426   Wiley

427 10. Kolotov VP, De Corte F (2004) Compilation of k_0 and related data for NAA in the
428   form of electronic database (IUPAC Technical Report). Pure Appl. Chem. 76:1921-
429   1925

430 11. Jovanovic S, Vukotic P, Smodis B, Jacimovic R, Mihaljevic N, Stegnar P (1989)

431 Epithermal neutron flux characterization of the TRIGA Mark II reactor, Ljubljana,

432 Yugoslavia, for use in NAA. J. Radioanal. Nucl. Chem. 129:343-349

433 12. JGCM 100:2008 (2008) Evaluation of measurement data - Guide to the expression of

434 uncertainty in measurement

435 13. Blachot J (2002) Nucl Data Sheets 95:679-836

436 14. Online available at http://www.ptb.de/emrp/sib09.html

Supplementary information

438 *Irradiation samples*

439

440 **Fig. S1** The precipitates in the upper part of the piled disks of the PE vials after drying

441 *Position of the radionuclide center of mass*

442 The distance between the radionuclide center of mass with respect to the center of the

443 8 mL PE vial, Δd, can be determined by using the following formula:

444
$$\frac{C_{rsu}(t_d)}{C_{usd}(t_d)} = \frac{1 - \dfrac{\Delta d}{d}}{1 + \dfrac{\Delta d}{d}},$$
(S1)

445 where $C_{rsu}(t_d)$, $C_{rsd}(t_d)$ are the count rates recorded with the right-side-up and up-side-

446 down sample, respectively, and d is the distance between the center of the 8 mL PE vial

447 and the (virtual) vertical position where the detector efficiency tends to infinite.